Supporting Information

Graphite carbon nitride doped with a benzene ring for enhanced photocatalytic H_2 evolution

Hai Yang Yuan,[a†] Jing Yang Bai,[a†] Beibei Xu,[b] Xin Yan Li,[a] Shi Yang Xiao,[a] Peng Fei Liu,[a] Xue Lu Wang,[b*] Hua Gui Yang[a*]

[a] Key Laboratory for Ultrafine Materials of Ministry of Education, Shanghai Engineering Research Center of Hierarchical Nanomaterials, School of Materials Science and Engineering, East China University of Science and Technology, 130 Meilong Road, Shanghai 200237, China.

[b] Physics Department & Shanghai Key Laboratory of Magnetic Resonance, School of Physics and Electronic Science, East China Normal University, Shanghai 200062, China.

† These authors contributed equally to this work.

* Corresponding authors: hgyang@ecust.edu.cn (H. G. Y), xlwang@phy.ecnu.edu.cn (X. L. Wang)

Experimental Section

Catalysts Preparation

Materials: All chemicals used in this study were analytical grade without further purification. The CN sample was carried out in a planetary ball-mill machine (QM-3SP2).

The preparation of CN samples: in the typical fabrication, 6.28 g of urea powders were added into an agate capsule containing agate balls of 5 mm in diameter (the ratio of ball to powder is 2:1). The above material was fixed in the planetary ball-mill machine and agitated with 400 rpm for 3 h. The milled powders were calcined in a corundum crucible, and then heated at a rate of 5 °C min^{-1} to reach the temperature of 550 °C and staged for 2 h. After cooling down to room temperature naturally, the as-prepared samples were ground into powder for further use.

The preparation of B-CN_{112} samples: 6.28 g of urea and 0.353 g of 1,3,5-tribromobenzene powders (0.112 mmol) were added into an agate capsule containing agate balls of 5 mm in diameter (the ratio of ball to powder is 2:1). The above materials were fixed in the planetary ball-mill machine and agitated with 400 rpm for 3 h. The milled powders were calcined in a corundum crucible, and then heated at a rate of 5 °C min^{-1} to reach the temperature of 550 °C and staged for 2 h. After cooling down to room temperature naturally, the as-prepared samples were ground into powder for further use. The B-CN_x samples were synthesized using the similar procedure except the adding amount of 1,3,5-tribromobenzene powders. For the sake of comparison, the urea with different weights of 1,3,5-tribromobenzene (0.176, 0.296 and 0.705 g) were prepared as the processing method described above and labeled as B-CN_{56}, B-CN_{94} and B-CN_{224}, respectively.

Characterization

X-ray diffraction analysis (XRD, D/MAX 2550 VB/PC) was collected to study the crystal structure. Infrared transmission was obtained with a Fourier transform infrared

(FTIR) spectrophotometer Spectrum (Nicolet). Element analysis was conducted by an elemental analyzer (vario ELII; Elementar Analysensyteme, Germany). The surface element contents and valence states were studied by XPS measurements (ESCALAB 250Xi). The C 1s peak at 284.8 eV was adopted as an internal reference in this work. The ^{13}C solid-state NMR experiments were performed on a Bruker AVANCE III 600 WB spectrometer operating at 600.44 MHz for 1H. Electron paramagnetic resonance (EPR) measurements were operated at EMX-8/2.7. The morphology and structure of as-prepared samples were characterized by scanning electron microscopy (SEM, HITACHI S4800) and transmission electron microscopy (TEM, JEM 2100, 200 kV). To investigate the light absorption of as-prepared samples, ultraviolet-visible (UV-vis) diffuse reflection spectra were carried out with a UV-vis spectrophotometer (CARY 500). To test the recombination of photoinduced electron-hole pairs, PL spectra were obtained by an Edinburgh Instruments (FLSP 920) system operated at room temperature.

Electrochemical impedance spectroscopy (EIS) measurements were conducted in a standard three electrode system with a CHI660E electrochemical workstation. The Pt mesh and Ag/AgCl electrode were used as the counter electrode and the reference electrode, respectively. Fluoride doped tin oxide (FTO) conductor glass with 1.0 cm^2 exposing area was used to prepare the working electrode. 10 mg catalyst was well dispersed in 50 μL Nafion solution and 100 μL dimethyl formamide (DMF). After ultrasonic treatment for 30 min, 20 μL slurry was dropped onto the prepared FTO glass and then dried naturally. We used 0.5 M Na_2SO_4 aqueous solution as the electrolyte. Transient photocurrent response measurements were performed under irradiation condition using a solar light simulator (Oriel, 91160, AM 1.5 globe) with light intensity of 100 mW cm^{-2} at a bias potential of -0.6 V vs. Ag/AgCl.

Photocatalytic activity evaluation

The solar-driven H_2-evolution reactions operated to estimate the activities of the

photocatalysts were carried out in a glass gas-closed circulation system (CEL-SPH2N, CEAU Light, China) with a top irradiation-type reaction vessel (LabSolar H_2). 3wt % Pt (H_2PtCl_6 as the precursor) as co-catalyst was loaded on the g-C_3N_4 through photo-deposition process. In a typical photocatalytic H_2 evolution reaction, 25 mg the prepared photocatalysts was dispersed in 50 mL of aqueous solution containing TEOA (10 % v/v) as hole scavenger. 300 W Xenon lamp (CEL-HXBF300) equipped with an ultraviolet cutoff filter was operated to provide visible light with ≥ 420 nm. The amount of evolved H_2 was analyzed by an online gas chromatograph/equipped with a TCD detector, using Ar carrier gas, and monitored every 30 min in order to determine the H_2 evolution rate. The suspension was put in ultrasonic bath for 5 min before the reaction. After evacuation by vacuum pump, air hardly can be detected in the system. The reaction started with mechanical stirring and the reactant solution was maintained at 10 °C by a flow of cooling water during the test. The AQY was measured under the wavelengths of 380, 405, 420, 435, 500, 550 and 600 nm band-pass filters for 1 h. To decide the photocatalytic stability of the sample, the long-term photocatalytic H_2 evolution experiment was conducted for 12 h. The experiments were carried out using a top-irradiation vessel containing 50 mL 10 vol % of TEOA aqueous solution. Photocatalyst power (25 mg) with 3 wt% Pt was used in the reaction. The AQY was then calculated by the following equation:

AQY (%) = 2×number of evolved H_2 molecules/number of incident photons×100%

Calculation Method

All calculations were carried out with the Gaussian 09 code,[1] in which the B3LYP hybrid density functional theory method was used.[2] The 6-31(d) basis set was used for all atoms, which has been applied in a similar system.[3] In our DFT calculation, the polarizable continuum model (PCM) was used to address solvent effects,[4] in which H_2O served as the solvent.

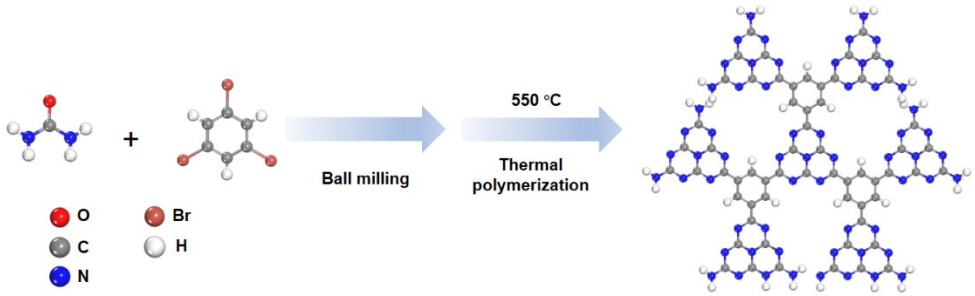

Fig. S1 The schematic synthesis illustration of benzene doped C_3N_4 with urea and tribromobenzene as precursors undergoing ball milling and thermal treatment.

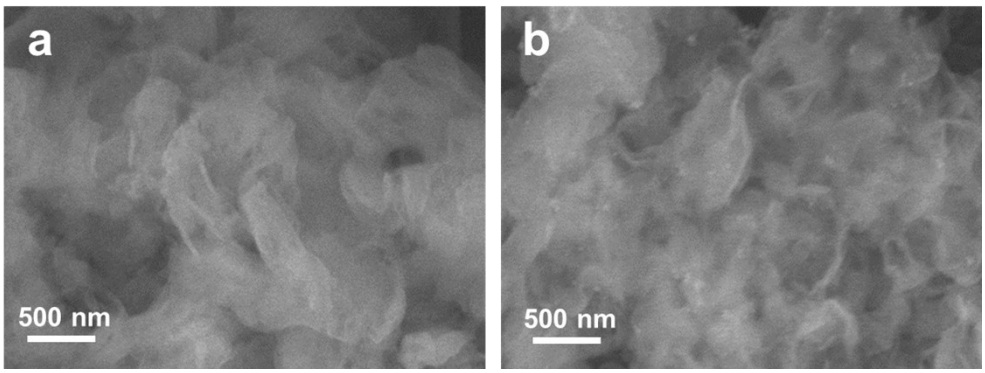

Fig. S2 The SEM images of (a) CN and (b) B-CN_{112}, respectively. Both samples display a light yarn shape, without obvious morphology changes.

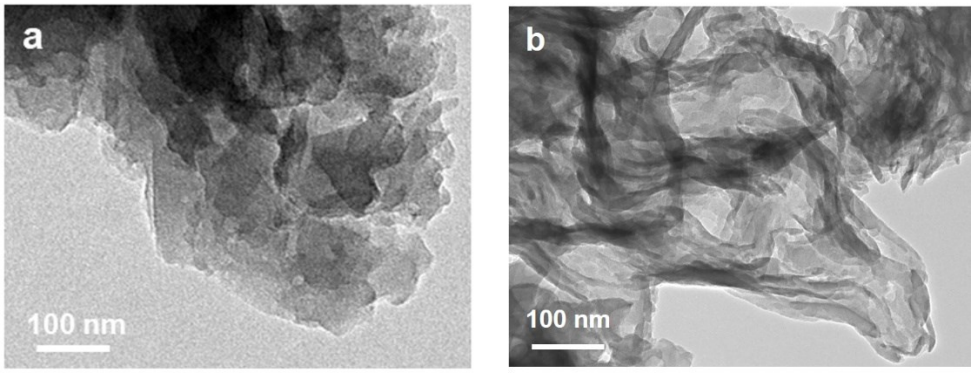

Fig. S3 The TEM images of (a) CN and (b) B-CN_{112}, respectively, showing a similar gossamer morphology.

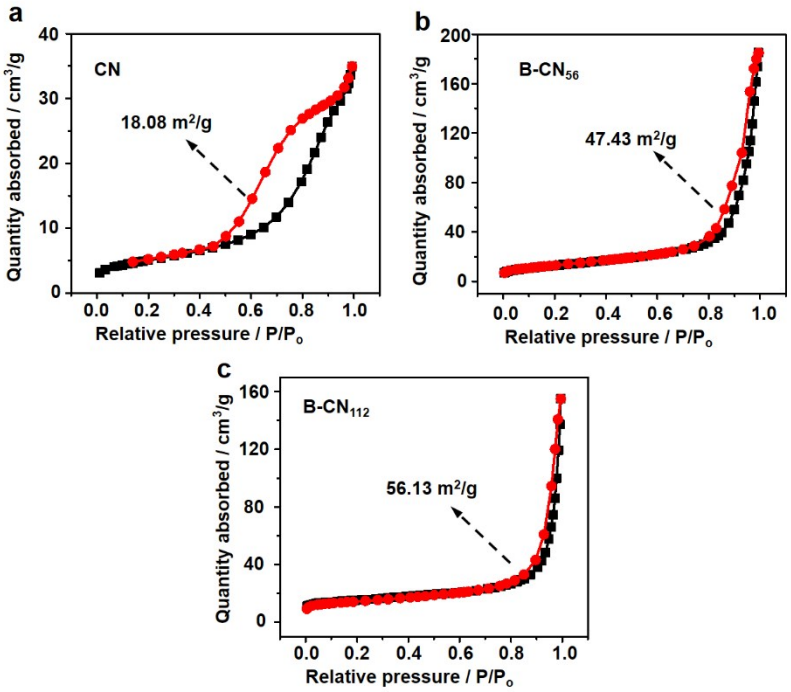

Fig. S4 N_2 adsorption-desorption isothermal curves of (a) CN, (b) B-CN_{56} and (c) B-CN_{112}, showing the increased specific surface areas caused by the easily-generated gases from the addition of $C_6H_3Br_3$ during the high-temperature polymerization process.

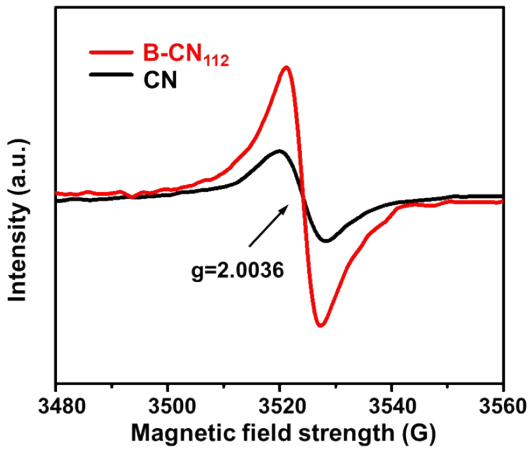

Fig. S5 Room temperature EPR spectra of CN and B-CN_{112} samples, exhibiting the increased peak intensity centered at g = 2.0036.

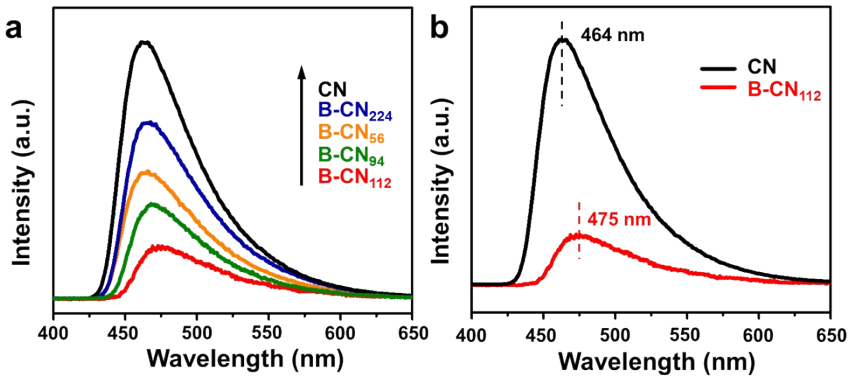

Fig. S6 The PL spectra of CN and B-CN_x (x = 56, 94, 112 and 224). The redshifted fluorescence peak of doped samples is consistent with the UV-vis spectra.

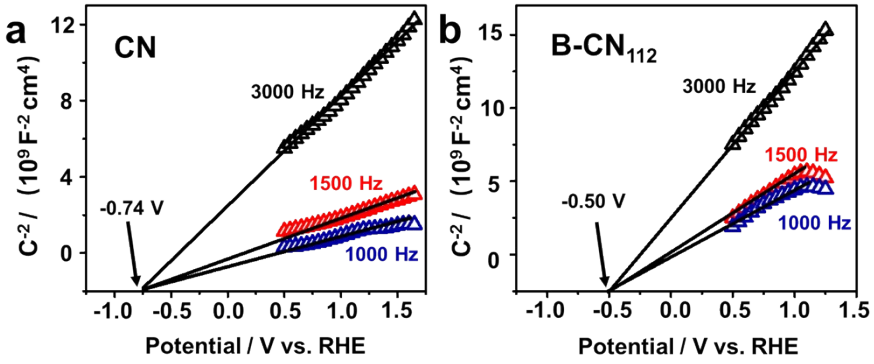

Fig. S7 Electrochemical Mott-Schottky plots at various frequencies of (a) CN and (b) B-CN_{112}, indicating the N-type feature for both samples.

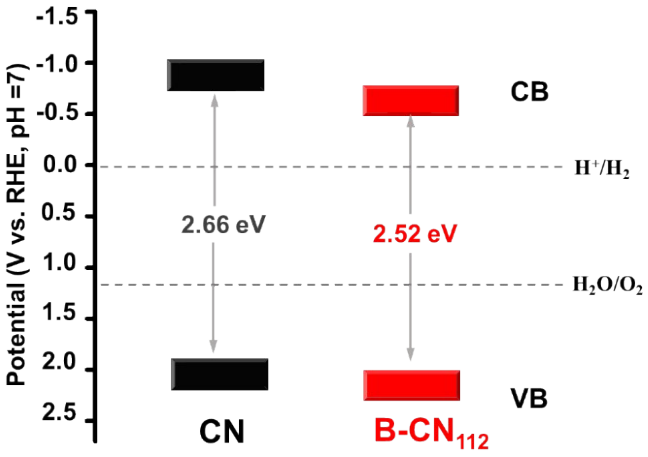

Fig. S8 Band alignment of CN and B-CN_{112}. All samples could satisfy the thermodynamic conditions for the photocatalytic splitting of water towards the H_2 evolution process.

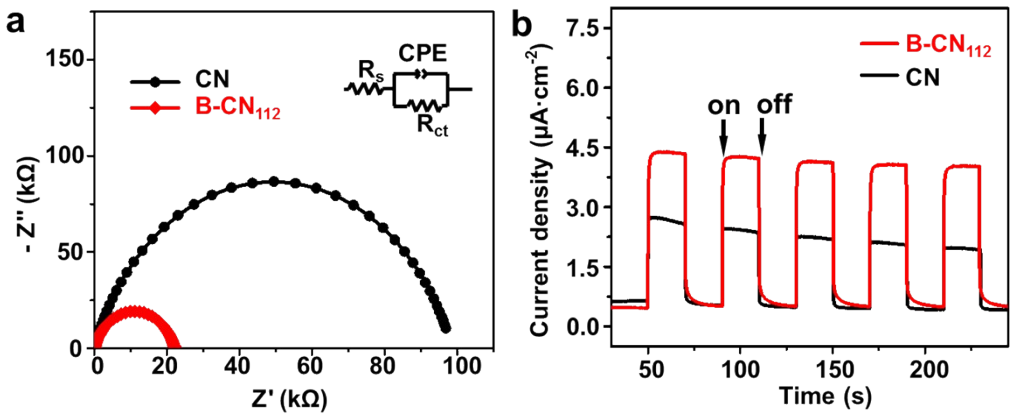

Fig. S9 (a) Electrochemical impedance spectra and (b) transient photocurrent response of CN and B-CN_{112}.

Table S1. Elemental analyses and corresponding C/N molar ratios.

Samples	N [wt%]	C [wt%]	C/N (atomic ratio)	H [wt%]
CN	60.61	34.16	0.6575	2.00
B-CN_{56}	60.82	34.55	0.6627	1.93
B-CN_{112}	59.27	35.21	0.6930	1.98
B-CN_{224}	58.43	35.96	0.7180	1.93

Table S2. Photocatalytic performance comparison of g-C_3N_4-based photocatalysts.

Materials	Activity under visible light ($\mu mol\ h^{-1}\ g^{-1}$)	Sacrificial agent	References
Benzene doped C_3N_4	**3360**	**TEOA**	**This work**
Uniform onion-ring-like g-C_3N_4/Pt	1900	TEOA	*ACS Nano*, 2018, **12**, 5551-5558[5]
Dopamine modified g-C_3N_4/Pt	1380	TEOA	*ACS Sustain. Chem. Eng.*, 2018, **6**, 8945-8953[6]
g-C_3N_4 with NaCl/KCl as high temperature solvent	13000	TEOA	*Angew. Chem. Int. Ed.*, 2019, **58**, 3433-3437[7]
Defects modified g-C_3N_4 nanosheets/Pt	613.4	TEOA	*Appl. Catal. B-Environ.*, 2018, **238**, 629-637[8]
N-deficient g-C_3N_4/Pt	2015	TEOA	*Appl. Catal. B-Environ.*, 2018, **238**, 465-470[9]
CeO_2/g-C_3N_4/Pt	1100	TEOA	*Appl. Catal. B-Environ.*, 2018, **238**, 111-118[10]
ZnS/g-C_3N_4/Pt	713.68	Na_2S and Na_2SO_3	*Appl. Catal. B-Environ.*, 2018, **229**, 41-51[11]
O-doped porous g-C_3N_4/Pt	1968	TEOA	*Appl. Catal. B-Environ.*, 2018, **221**, 9-16[12]
Oxygen-containing groups-modified g-C_3N_4/Pt	752	Lactic acid	*Appl. Surf. Sci.*, 2018, **427**, 645-653[13]
Hollow-nanosphere based mesoporous g-C_3N_4/Pt	659.8	TEOA	*Appl. Surf. Sci.*, 2018, **455**, 591-598[14]
Non-metal group doped porous ultrathin g-C_3N_4 nanosheets/Pt	1323.5	TEOA	*Nanoscale*, 2018, **10**, 5239-5245[15]
Oxygen self-doped g-C_3N_4	3174	TEOA	*Nanoscale*, 2018, **10**, 4515-4522[16]
2D/2D transition-metal-oxide/g-C_3N_4 Z-scheme heterojunction	37000	TEOA	*ACS Nano*, 2019, **13**, 11294-11302[17]
3D porous P-doped g-C_3N_4 tube/Pt	2020	TEOA	*Appl. Catal. B-Environ.*, 2019, **241**, 159-166[18]
S, P, O codoped ultrathin g-	2480	TEOA	*Appl. Catal. B-Environ.*, 2019, **248**, 84-94[19]

C_3N_4 nanosheets/Pt			
Ultrathin 2D/2D WO_3/g-C_3N_4/Pt	982	Lactic acid	*Appl. Catal. B-Environ.*, 2019, **243**, 556-565[20]
Nitrogen vacancies modified g-C_3N_4/Pt	8171.4	TEOA	*Chem. Eng. J.*, 2019, **358**, 20-29[21]
Oxamide-modified g-C_3N_4/Pt	1540	TEOA	*Chem. Eng. J.*, 2019, **374**, 1064-1075[22]
Porous g-C_3N_4 nanosheets/Pt	115.5	TEOA	*Nano Energy*, 2019, **59**, 598-609[23]
$BiPO_4$/S-doped g-C_3N_4/Pt	1170	TEOA	*ACS Appl. Energy Mater.*, 2020, **3**, 5024-5030[24]
Melamine Functionalized 2D g-C_3N_4 poly (heptazine imide)	5570	Methanol and TEOA	*Adv. Energy Mater.*, 2021, DOI: 10.1002/aenm.202003016[25]
g-C_3N_4/Cu single atom	10600	Methanol	*Adv. Mater.*, 2020, **32**, 2003082[26]
$NaHCO_3$ template Porous crystalline g-C_3N_4/Pt	1010	Lactic acid	*Appl. Catal. B-Environ.*, 2020, **271**, 118899[27]
$Ba_5Nb_4O_{15}$/g-C_3N_4	2670	Oxalic acid	*Appl. Catal. B-Environ.*, 2020, **263**, 117730[28]
Functionalized monolayer g-C_3N_4/Pt	29300	TEOA	*Appl. Catal. B-Environ.*, 2020, **260**, 118181[29]
Ultrathin Porous g-C_3N_4 Bundles	4765	TEOA	*Angew. Chem. Int. Ed.*, 2021, DOI: 10.1002/anie.202013753[30]
Tandem 0D/2D/2D NbS_2 quantum dot/Nb_2O_5 nanosheet/g-C_3N_4 flake	7300	TEOA	*Small*, 2020, **16**, 2003302[31]
Rapid polymerization high crystalline g- C_3N_4/Pt	320	TEOA	*Int. J. Hydrogen Energy*, 2020, **45**, 6425-6436[32]
Holey g-C_3N_4 nanosheets/Pt	2320	TEOA	*Appl. Catal. B-Environ.*, 2021, **283**, 119637[33]

Notes: The activities mentioned above were all calculated based on the hydrogen evolution amount of the 1st hour's test.

Reference

[1] M. J. E. A. Frisch, G. W. Trucks, H. B. Schlegel, G. E. Scuseria, M. A. Robb, J. R. Cheeseman, G. Scalmani, V. Barone, B. Mennucci, G. A. Petersson, H. Nakatsuji, et al., Gaussian 09, Revision A.02; Gaussian, Inc., Wallingford, CT, 2009.

[2] A. D. Becke, *J. Chem. Phys.,* 1993, **98**, 5648.

[3] H. Gao, Y. Guo, Z. Yu, M. Zhao, Y. Hou, Z. Zhu, S. Yan, Q. Liu, Z. Zou, *ChemSusChem,* 2019, **12**, 4285.

[4] J. Tomasi, B. Mennucci, R. Cammi, *Chem. Rev.*, 2005, **105**, 2999.

[5] L. Cui, J. Song, A. F. McGuire, S. Kang, X. Fang, J. Wang, C. Yin, X. Li, Y. Wang and B. Cui, *ACS Nano*, 2018, **12**, 5551-5558.

[6] P. Xia, M. Liu, B. Cheng, J. Yu and L. Zhang, *ACS Sustain. Chem. Eng.*, 2018, **6**, 8945-8953.

[7] G. Zhang, G. Li, T. Heil, S. Zafeiratos, F. Lai, A. Savateev, M. Antonietti and X. Wang, *Angew. Chem. Int. Ed.*, 2019, **58**, 3433-3437.

[8] J. Wang, Z. Yang, W. Yao, X. Gao and D. Tao, *Appl. Catal. B-Environ.*, 2018, **238**, 629-637.

[9] J. Liu, W. Fang, Z. Wei, Z. Qin, Z. Jiang and W. Shangguan, *Appl. Catal. B-Environ.*, 2018, **238**, 465-470.

[10] W. Zou, B. Deng, X. Hu, Y. Zhou, Y. Pu, S. Yu, K. Ma, J. Sun, H. Wan and L. Dong, *Appl. Catal. B-Environ.*, 2018, **238**, 111-118.

[11] X. Hao, J. Zhou, Z. Cui, Y. Wang, Y. Wang and Z. Zou, *Appl. Catal. B-Environ.*, 2018, **229**, 41-51.

[12] J.-W. Zhang, S. Gong, N. Mahmood, L. Pan, X. Zhang and J.-J. Zou, *Appl. Catal. B-Environ.*, 2018, **221**, 9-16.

[13] X. Wu, F. Chen, X. Wang and H. Yu, *Appl. Surf. Sci.*, 2018, **427**, 645-653.

[14] Z. Zhao, X. Wang, Z. Shu, J. Zhou, T. Li, W. Wang and Y. Tan, *Appl. Surf. Sci.*, 2018, **455**, 591-598.

[15] W. Xing, G. Chen, C. Li, Z. Han, Y. Hu and Q. Meng, *Nanoscale*, 2018, **10**, 5239-

5245.

[16] F. Wei, Y. Liu, H. Zhao, X. Ren, J. Liu, T. Hasan, L. Chen, Y. Li and B. L. Su, *Nanoscale*, 2018, **10**, 4515-4522.

[17] H. Xu, X. She, T. Fei, Y. Song, D. Liu, H. Li, X. Yang, J. Yang, H. Li, L. Song, P. M. Ajayan and J. Wu, *ACS Nano*, 2019, **13**, 11294-11302.

[18] M. Wu, J. Zhang, B.-b. He, H.-w. Wang, R. Wang and Y.-s. Gong, *Appl. Catal. B-Environ.*, 2019, **241**, 159-166.

[19] Q. Liu, J. Shen, X. Yu, X. Yang, W. Liu, J. Yang, H. Tang, H. Xu, H. Li, Y. Li and J. Xu, *Appl. Catal. B-Environ.*, 2019, **248**, 84-94.

[20] J. Fu, Q. Xu, J. Low, C. Jiang and J. Yu, *Appl. Catal. B-Environ.*, 2019, **243**, 556-565.

[21] J. Wu, N. Li, H.-B. Fang, X. Li, Y.-Z. Zheng and X. Tao, *Chem. Eng. J.*, 2019, **358**, 20-29.

[22] H. Tang, R. Wang, C. Zhao, Z. Chen, X. Yang, D. Bukhvalov, Z. Lin and Q. Liu, *Chem. Eng. J.*, 2019, **374**, 1064-1075.

[23] X. Gao, J. Feng, D. Su, Y. Ma, G. Wang, H. Ma and J. Zhang, *Nano Energy*, 2019, **59**, 598-609.

[24] D. Long, Z. Chen, X. Rao and Y. Zhang, *ACS Appl. Energy Mater.*, 2020, **3**, 5024-5030.

[25] J. Kröger, A. Jiménez-Solano, G. Savasci, P. Rovó, I. Moudrakovski, K. Küster, H. Schlomberg, H. A. Vignolo-González, V. Duppel, L. Grunenberg, C. B. Dayan, M. Sitti, F. Podjaski, C. Ochsenfeld and B. V. Lotsch, *Adv Energy Mater.*, **2021**, DOI: 10.1002/aenm.202003016.

[26] X. Xiao, Y. Gao, L. Zhang, J. Zhang, Q. Zhang, Q. Li, H. Bao, J. Zhou, S. Miao, N. Chen, J. Wang, B. Jiang, C. Tian and H. Fu, *Adv. Mater.*, 2020, **32**, 2003082.

[27] X. Wu, H. Ma, W. Zhong, J. Fan and H. Yu, *Appl. Catal. B-Environ.*, 2020, **271**, 118899.

[28] K. Wang, Y. Li, J. Li and G. Zhang, *Appl. Catal. B-Environ.*, 2020, **263**, 117730.

[29] L. Jiang, J. Li, K. Wang, G. Zhang, Y. Li and X. Wu, *Appl. Catal. B-Environ.*, 2020, **260**, 118181.

[30] B. Wu, L. Zhang, B. Jiang, Q. Li, C. Tian, Y. Xie, W. Li and H. Fu, *Angew. Chem. Int. Ed.* 2021, DOI: 10.1002/anie.202013753.

[31] B. Lin, Z. Chen, P. Song, H. Liu, L. Kang, J. Di, X. Luo, L. Chen, C. Xue, B. Ma, G. Yang, J. Tang, J. Zhou, Z. Liu and F. Liu, *Small*, 2020, **16**, 2003302.

[32] L. Wang, Y. Hong, E. Liu, Z. Wang, J. Chen, S. Yang, J. Wang, X. Lin and J. Shi, *Int. J. Hydrogen Energy*, 2020, **45**, 6425-6436.

[33] G. Li, Z. Xie, S. Chai, X. Chen and X. Wang, *Appl. Catal. B-Environ.*, 2021, **283**, 119637.